Vibronic spectra in condensed matter: A comparison of exact quantum mechanical and various semiclassical treatments for harmonic baths

S. A. Egorov, Eran Rabani, and B. J. Berne
Department of Chemistry, Columbia University, 3000 Broadway, New York, New York 10027

(Received 28 August 1997; accepted 7 October 1997)

We consider the problem of calculating the vibronic absorption spectrum of a diatomic molecule coupled to a condensed phase environment, where all nuclear degrees of freedom are taken in the quadratic approximation, and where the two electronic states couple differently to the solvent. This simple model is used to examine several commonly used semiclassical approximations. The method of Kubo–Toyozawa is adapted to enable exact calculation of the real-time dipole autocorrelation function for the quantum mechanical treatment. Alternatively, we derive an expression for this correlation function in terms of a path-integral influence functional, which is not limited to a finite number of bath modes and could be applied to treat anharmonic solutes in condensed matter. We then obtain an analytical solution for the classical treatment of nuclear dynamics, and develop a mixed quantum-classical approach, where the dynamics of the diatomic vibrational mode is treated quantum mechanically and the bath is treated classically. It is shown that the mixed quantum-classical treatment provides better agreement with the exact quantum treatment than the other approximations for a wide range of parameters. Exact analytical results similar to the pure dephasing theory of Skinner and Hsu are obtained for the asymptotic long time behavior of the dipole autocorrelation functions. © *1998 American Institute of Physics.* [S0021-9606(98)50303-0]

I. INTRODUCTION

A molecular system coupled to a bath serves as a prototype model for studying numerous physical and chemical processes in condensed phases. One particular example is provided by the electronic spectroscopy of chromophores in crystalline or liquid hosts.[1–3] The effect of nuclear dynamics of the bath particles on the line shape reveals itself in the shift and broadening of individual spectral lines comprising the gas phase electronic absorption spectrum of the chromophore. As such, the absorption spectrum of a molecule embedded in a crystal or in a liquid provides valuable information about the structure and dynamics of the host and the chromophore perturbed by the host.

Quantum mechanical calculations of electronic absorption spectra in condensed phases are extremely difficult in view of the large number of degrees of freedom involved. For any realistic system this many-body problem can only be solved approximately. One common approach is to use path integral Monte Carlo techniques[4,5] to obtain the imaginary-time dipole autocorrelation function and to analytically continue it to real time, using maximum entropy methods[6–8] or singular value decomposition.[9,10] An alternative approach is to use a time-dependent Hartree method, which assumes factorization of the multi-dimensional wave function into a product of one particle wave functions.[11] As such, this approach is limited to relatively weak system-bath coupling. Evans and Coalson[12] have adapted the cumulant expansion based method due to Nitzan and Silbey,[13] to obtain an absorption spectrum of a general system coupled to an arbitrary bath. They compared this latter approach to the time-dependent Hartree method and found significant improvement. However, the method involves truncation of the time evolution operator after the second order term in the system-bath interaction, and as such is not free of limitations either.

Another possibility is to restrict the quantum mechanical treatment to a few selected ‘‘highly’’ quantum degrees of freedom of the primary system, while adopting some kind of classical approximation in treating the bath dynamics. The simplest approximation would be to retain the quantum nature of the electronic degrees of freedom only, and to treat all nuclear degrees of freedom (including those of the chromophore) classically.[14–18] When the nuclear coordinates of the primary system are strongly perturbed by the electronic transition, it would seem appropriate to extend the quantum methodology to these degrees of freedom, and to couple their quantum dynamics in some way to the classical dynamics of the bath particles.[19,20] A long-standing problem is how to simulate transitions between different electronic states induced by the nuclear motion in arbitrary condensed matter systems.[21–27] Of particular relevance for the present study is the work of Thirumalai, Bruskin and Berne,[28] who extended the Gaussian wave-packet method[29–31] to determine the electronic spectra of a diatomic molecule embedded in a rare gas matrix.

All types of the mixed quantum-classical calculations mentioned above inevitably introduce uncontrolled approximations, and are not guaranteed to give accurate results for the state-to-state transition probabilities. For example, it is now known for vibrational relaxation[32,33] that if the solute vibration is treated quantum mechanically and the bath is treated classically, very serious errors occur in the transition rate (up to 20 orders of magnitude). For electronic transitions, on the other hand, it may well be the case that a classical bath approximation is still valid under some circumstances. In view of this, it would be important to assess the accuracy of the different mixed quantum-classical treatments; hence we consider a simple model for which a fully quantum mechanical as well as various semiclassical solutions are obtained analytically.

We study the electronic absorption spectrum of a diatomic molecule embedded in a condensed phase environment. The vibrational mode of the molecule is treated in the harmonic approximation and the host is modeled by a harmonic bath. The coupling between the diatomic and the bath is taken to be linear both in the molecule and in the bath vibrational coordinates. The electronic transition of the diatomic molecule from the ground to the excited state is accompanied by a change in the equilibrium position of its vibrational mode, in the vibrational frequency of this mode, and in the strength of its coupling to the bath. This model is general enough to capture the essential features of the electronic absorption spectrum, yet as will be shown below it is simple enough to be analytically solvable—both quantum mechanically and in the various semiclassical approximations described in this work. In particular, for a finite number of bath modes we obtain exact numerical results for the dipole autocorrelation functions at all times, and concomitantly, through its Fourier transform the vibronic absorption spectra. A similar model has been extensively studied by Skinner and Hsu[34,35] in the context of the pure dephasing problem, where the primary interest is in the asymptotic long time behavior of the dipole autocorrelation function, which determines the frequency shifts and the dephasing rates. We adapt the theory developed by Skinner and Hsu[34,35] to the present problem and obtain exact analytic results for the frequency shifts and the dephasing rates both for the case when all nuclear dynamics are treated either quantum mechanically or classically. For a particular case of zero system-bath coupling in the diatomic ground electronic state, but non-zero couplings in the excited electronic state, we also obtain the asymptotic results for the mixed quantum-classical case (quantum diatomic vibrational mode–classical bath). In this case we find that the mixed treatment represents a significant improvement over the fully classical treatment of nuclear dynamics.

The outline of the paper is as follows. In Section II we define our model Hamiltonian and present the expression for the electronic absorption spectrum in terms of the real-time dipole autocorrelation function. In Section III we obtain analytical expressions for the fully quantum mechanical and various semiclassical approximations for this autocorrelation function. In Section IV we study its asymptotic long time behavior, which allows us to obtain analytical results for the dephasing rates and frequency shifts. The numerical results for the dipole autocorrelation functions and for the spectra are given in Section V along with the theoretical predictions of the dephasing rates and the frequency shifts. Finally, in Section VI we conclude.

II. MODEL SYSTEM AND ABSORPTION SPECTRUM

In this section we define the model system and outline the methodology to compute the absorption spectrum.

A. Model Hamiltonian and spectral density

The model described here is a simple one and can be solved exactly. We consider a diatomic molecule coupled to a bath and focus on a particular pair of electronic states of the diatomic molecule, which give rise to the electronic transition, when the diatomic molecule goes from its ground electronic state (denoted by $|0\rangle$) to the excited electronic state (denoted by $|1\rangle$). We approximate the internal vibrational degree of freedom by a harmonic mode and fix the orientation of the molecule. The bath is modeled by an ensemble of harmonic oscillators. The coupling between the internal vibrational mode of the diatomic molecule and the bath is bilinear, but the coupling coefficients are different for the two electronic states. For simplicity, we neglect off-diagonal terms that couple the bath and the two electronic states, since we are interested in the pure dephasing process, which is on a much faster time scale than the electronic population relaxation.

In the Born–Oppenheimer approximation, the total Hamiltonian can be written as

$$H=H_0|0\rangle\langle 0|+H_1|1\rangle\langle 1|, \tag{1}$$

where H_0 (H_1) is the Hamiltonian for the nuclear degrees of freedom of the system and the bath, corresponding to the motion on the Born–Oppenheimer potential surface when the diatomic molecule is in its ground (or excited) electronic states.

The ground and excited state Hamiltonians are:

$$H_0=h_0(q)+H_b(\mathbf{Q})+V_0(q,\mathbf{Q}), \tag{2}$$

and

$$H_1=h_1(q)+H_b(\mathbf{Q})+V_1(q,\mathbf{Q})+\hbar\omega_e. \tag{3}$$

In Eq. (3) $\hbar\omega_e$ is the gas phase electronic transition energy of the diatomic molecule (for convenience we set it equal to 0). $h_0(q)$ and $h_1(q)$ are the Hamiltonian for the vibrational coordinate of the diatomic molecule when it is in its ground ($|0\rangle$) or excited ($|1\rangle$) electronic states, respectively,

$$h_{0,1}(q)=\tfrac{1}{2}p^2+\tfrac{1}{2}\omega_{0,1}^2(q-q_{0,1})^2, \tag{4}$$

where q is the diatomic mass-weighted vibrational coordinate with a conjugate momentum p, frequency ω_0 and equilibrium position q_0 for state $|0\rangle$ and frequency ω_1 and equilibrium position q_1 for state $|1\rangle$.

The bath Hamiltonian in the harmonic approximation takes the form

$$H_b(\mathbf{Q})=\frac{1}{2}\sum_{\alpha}^{N_b}P_\alpha^2+\frac{1}{2}\sum_{\alpha}^{N_b}\omega_\alpha^2Q_\alpha^2, \tag{5}$$

where the summation index α labels the bath mass weighted coordinates Q_α with conjugate momenta P_α, and frequencies ω_α; N_b is the number of bath modes.

As mentioned earlier, the system-bath coupling is taken to be linear both in the system and in the bath coordinates

$$V_{0,1}(q,\mathbf{Q})=\sum_{\alpha}^{N_b}g_\alpha^{0,1}(q-q_{0,1})Q_\alpha, \tag{6}$$

where g_α^0 (g_α^1) are the coupling strengths for the ground (excited) electronic states, which we assume to be *different* for the two electronic states of the diatomic molecule.

The effect of the bath on the system is completely determined by the two spectral densities, one for the ground electronic state

$$J_0(\omega)=\sum_\alpha^{N_b} \frac{(g_\alpha^0)^2}{2\omega_\alpha}\delta(\omega-\omega_\alpha), \tag{7}$$

and the other for the excited electronic state

$$J_1(\omega)=\sum_\alpha^{N_b} \frac{(g_\alpha^1)^2}{2\omega_\alpha}\delta(\omega-\omega_\alpha). \tag{8}$$

The theory presented here can accommodate different functional forms for the two spectral densities. However, for simplicity we use the same functional form for $J_0(\omega)$ and for $J_1(\omega)$. However, the two functions are normalized to different values (ρ_0 and ρ_1, respectively) which indicates the difference in the overall system-bath coupling strength.

The formulation below holds for an arbitrary choice of the functional form of the spectral density. However, here we will restrict ourselves to the treatment of monatomic hosts in which case we will only consider acoustic phonons. The extension to optical phonons is straightforward. The conventional choice of spectral density for acoustic phonons is the Debye model coupled with the deformation potential approximation.[36] This gives a spectral density which is proportional to ω^3, and has a sharp cutoff at the Debye frequency. For numerical convenience the model can be slightly modified[12] by introducing a smooth exponential cutoff

$$J_{0,1}(\omega)=\rho_{0,1}\frac{\gamma^4}{6}\omega^3\ \exp(-\gamma\omega). \tag{9}$$

For liquid hosts, one has to consider a different functional form for the spectral densities.[33,37]

Having defined the Hamiltonian and the spectral density we can proceed to the discussion of the calculation of the absorption spectrum in the following subsection.

B. Vibronic absorption spectrum

We calculate the electronic spectrum within the Fermi golden rule and the electric dipole approximation.[38] The normalized electronic absorption spectrum is given by the Fourier transform of the real-time dipole autocorrelation function:

$$I(\omega)=\frac{1}{2\pi}\int_{-\infty}^{\infty}dt\ \exp(i\omega t)C(t), \tag{10}$$

where the real-time dipole autocorrelation function is given by

$$C(t)=\frac{\mathrm{Tr}[e^{-\beta H}e^{iHt/\hbar}\mu e^{-iHt/\hbar}\mu]}{\mathrm{Tr}[e^{-\beta H}\mu^2]}, \tag{11}$$

$\beta=1/k_BT$, $\mathrm{Tr}(\cdots)$ denotes the trace over all nuclear and electronic degrees of freedom, and μ is the transition-dipole operator.

Within the Condon approximation μ does not depend on the nuclear coordinates. Hence we replace the transition-dipole operator with

$$\mu=\mu_{01}|0\rangle\langle 1|+\mu_{10}|1\rangle\langle 0|. \tag{12}$$

We will limit the discussion to temperatures much lower than the electronic energy gap ($\hbar\omega_e \gg kT$). Carrying out the trace over the electronic states results in

$$C(t)=\langle e^{iH_0t/\hbar}e^{-iH_1t/\hbar}\rangle, \tag{13}$$

In the above $\langle\cdots\rangle=\mathrm{Tr}_{\mathbf{x}}(\rho_0\cdots)$ denotes the trace only over the nuclear coordinates and $\mathbf{x}\equiv(q,\mathbf{Q})$. The equilibrium density operator is given by

$$\rho_0=e^{-\beta H_0}/Z(\beta), \tag{14}$$

where $Z(\beta)$ is the partition function

$$Z(\beta)=\mathrm{Tr}_{\mathbf{x}}[e^{-\beta H_0}]=\int d\mathbf{x}\langle\mathbf{x}|e^{-\beta H_0}|\mathbf{x}\rangle. \tag{15}$$

For future purposes (in order to discuss the various semiclassical limits of the absorption spectrum) we present two alternative forms for $C(t)$ in Eq. (13). The first form employs a time-ordered exponential[14,39]

$$C(t)=\left\langle \exp_{\vec{T}}\left\{-\frac{i}{\hbar}\int_0^t dt'\Delta(t')\right\}\right\rangle, \tag{16}$$

where $\vec{T}$ is the time ordering operator which places $\Delta(t)$ in the order decreasing time from left to right. In the above $\Delta(t)$ is the Heisenberg form of the operator Δ given by

$$\Delta(t)=e^{iH_0t/\hbar}\Delta e^{-iH_0t/\hbar}, \tag{17}$$

and Δ is the difference between the excited and ground state Hamiltonians

$$\Delta=H_1-H_0. \tag{18}$$

The second alternative form for $C(t)$ is based on the semiclassical theory of Shemetulskis and Loring,[16] which rewrites $C(t)$ in terms of phase space integrals using the Wigner distribution.[40] $C(t)$ then takes the following form:

$$C(t)=\int d\mathbf{p}_{\mathbf{x}}\int d\mathbf{x}W(\mathbf{p}_{\mathbf{x}},\mathbf{x},t), \tag{19}$$

where $W(\mathbf{p}_{\mathbf{x}},\mathbf{x},t)$ satisfies

$$\dot{W}(\mathbf{p}_{\mathbf{x}},\mathbf{x},t)=-\mathcal{L}W(\mathbf{p}_{\mathbf{x}},\mathbf{x},t). \tag{20}$$

In the above, the operator $\mathcal{L}$ is given by

$$\mathcal{L}=-\frac{i}{\hbar}\Delta\ \cos(\hbar\hat{\Lambda}/2)+\frac{2}{\hbar}H_{\mathrm{av}}\ \sin(\hbar\hat{\Lambda}/2), \tag{21}$$

where $\hat{\Lambda}$ is the Poisson bracket operator

$$\hat{\Lambda}\equiv\overleftarrow{\nabla}_{\mathbf{p}_{\mathbf{x}}}\cdot\overrightarrow{\nabla}_{\mathbf{x}}-\overleftarrow{\nabla}_{\mathbf{x}}\cdot\overrightarrow{\nabla}_{\mathbf{p}_{\mathbf{x}}}, \tag{22}$$

and where the right and left arrows on the differential operator indicate that the operator acts on functions which are on the right or on the left with respect to the operator. The operator Δ is defined in Eq. (18) and H_{av} is the arithmetic averaged Hamiltonian

$$H_{\mathrm{av}}=\tfrac{1}{2}(H_0+H_1). \tag{23}$$

Both quantum mechanical forms of the real-time dipole autocorrelation function are essentially equivalent. However, the semiclassical limit ($\hbar\rightarrow 0$) of these is not unique.[14] This arises because the two electronic states are treated quantum mechanically, while the nuclear degrees of freedom are treated classically. We will return to this point below when we discuss the semiclassical limits of $C(t)$ and will make the connection between the semiclassical limits of the two forms given above.

III. REAL-TIME DIPOLE AUTOCORRELATION FUNCTIONS

Within the Fermi golden rule, the real-time dipole autocorrelation functions for the harmonic model can be calculated exactly. Here, we will obtain the analytical solution for $C(t)$ for three cases.

(a) The fully quantum mechanical (FQM) results are calculated by employing the density matrix formalism of Kubo and Toyozawa,[41] which is based on Gaussian integrals. (Equivalently we have also used the boson algebra technique of Balian and Brezin,[42] which allows evaluation of the thermal averages of exponentiated quadratic functions of phonon operators.) In either case, the calculation can be done only for a finite number of bath modes.

(b) A semiclassical approximation in which the dynamics of all nuclear degrees of freedom (diatomic molecule and host) are treated classically, while preserving the quantum mechanical nature of the electronic transition. Two alternative classical propagation schemes have been studied. The first assumes that all dynamical classical variables are propagated using the ground state Hamiltonian. We will refer to this approximation as the dynamical classical limit (DCL). The second, which is derived from Eq. (19), assumes that all dynamical classical variables are propagated using the arithmetic averaged Hamiltonian. We will refer to this approximation as the averaged classical limit (ACL). Both limits have been extensively discussed by Mukamel[14] for the simpler case of an isolated molecular system, but as far as we know, have never been carried out analytically for a molecular system coupled to a bath, where the coupling strength is different in the two electronic state (i.e. $J_0(\omega)\neq J_1(\omega)$). As a by-product, we also obtain the static classical limit (SCL), which yields the well-known classical Franck–Condon spectrum.[43]

(c) A mixed ensemble in which the primary (diatomic) vibrational coordinate is treated quantum mechanically, while the bath is treated in the dynamical classical limit. We will refer to this approach as the mixed quantum-classical limit (MQC). The effect of the bath on the spectrum in this approach is entirely given by the influence functional of Feynman and Vernon,[44] which is generalized for the present problem. As such, this method is not limited to a finite number of bath modes. In addition, it could be extended to the study of anharmonic molecular systems bilinearly coupled to a harmonic bath.

A. The fully quantum mechanical *C*(*t*)

The Kubo–Toyozawa[41] method is used to calculate the full time dependence of the quantum mechanical dipole autocorrelation function (we have also used the algebraic operator approach[42] as a check of the results). For the sake of completeness we outline Kubo–Toyozawa derivation for the problem at hand. In the coordinate representation Eq. (13) takes the form

$$C_{\mathrm{FQM}}(t)=\int d\mathbf{x}d\mathbf{x}'K_0(\mathbf{x},\mathbf{x}')K_1(\mathbf{x},\mathbf{x}')/Z(\beta), \tag{24}$$

where $K_0(\mathbf{x},\mathbf{x}')$ is the forward propagator

$$K_0(\mathbf{x},\mathbf{x}')=\langle\mathbf{x}|e^{-(\beta-it/\hbar)H_0}|\mathbf{x}'\rangle, \tag{25}$$

and $K_1(\mathbf{x},\mathbf{x}')$ is the backward propagator

$$K_1(\mathbf{x},\mathbf{x}')=\langle\mathbf{x}'|e^{-itH_1/\hbar}|\mathbf{x}\rangle. \tag{26}$$

The tensor expression for the off-diagonal element of the density operator/propagator in the coordinate representation for the collection of coupled harmonic oscillators is given by Kubo and Toyozawa:

$$\begin{aligned}K_0(\mathbf{x},\mathbf{x}')=&[\det(2\pi\hbar\Omega_0^{-1}\sinh\{(\beta\hbar-it)\Omega_0\})]^{-1/2}\\&\times\exp[-\tfrac{1}{4}(\mathbf{x}+\mathbf{x}'-2\mathbf{x}_0)^T\{\hbar^{-1}\Omega_0\\&\times\tanh((\beta\hbar-it)\Omega_0/2)\}(\mathbf{x}+\mathbf{x}'-2\mathbf{x}_0)\\&-\tfrac{1}{4}(\mathbf{x}-\mathbf{x}')^T\{\hbar^{-1}\Omega_0\coth((\beta\hbar-it)\Omega_0/2)\}\\&\times(\mathbf{x}-\mathbf{x}')].\end{aligned} \tag{27}$$

In the above Ω_0^2 is the (square) force constant matrix of rank N for the ground electronic state, where $N=N_b+1$ is the total number of vibrational modes. The nuclear potential energy of the ground state (U_0) can be expressed in terms of Ω_0^2 as follows:

$$\begin{aligned}U_0&=\frac{1}{2}\omega_0^2(q-q_0)^2+\frac{1}{2}\sum_{\alpha}^{N_b}\omega_\alpha^2Q_\alpha^2+\sum_{\alpha}^{N_b}g_\alpha^0(q-q_0)Q_\alpha\\&=\frac{1}{2}(\mathbf{x}-\mathbf{x}_0)^T\Omega_0^2(\mathbf{x}-\mathbf{x}_0).\end{aligned} \tag{28}$$

In what follows, we set $\mathbf{x}_0=\mathbf{0}$ without loss of generality. Analogously, $K_1(\mathbf{x},\mathbf{x}')$ is expressed in terms of the force constant matrix Ω_1^2 ($N\times N$) for the excited electronic state with the nuclear potential energy U_1,

$$\begin{aligned}U_1&=\frac{1}{2}\omega_1^2(q-q_1)^2+\frac{1}{2}\sum_{\alpha}^{N_b}\omega_\alpha^2Q_\alpha^2+\sum_{\alpha}^{N_b}g_\alpha^1(q-q_1)Q_\alpha\\&=\frac{1}{2}(\mathbf{x}-\mathbf{x}_1)^T\Omega_1^2(\mathbf{x}-\mathbf{x}_1).\end{aligned} \tag{29}$$

Using the results for the two propagators $K_0(\mathbf{x},\mathbf{x}')$ and $K_1(\mathbf{x},\mathbf{x}')$, the integration over $\mathbf{x}$ and $\mathbf{x}'$ in Eq. (24) can be easily performed to yield the following result for $C_{\mathrm{FQM}}(t)$:

$$C_{\mathrm{FQM}}(t)=e^{-S_{\mathrm{FQM}}(t)}e^{-R_{\mathrm{FQM}}(t)}e^{-i\omega_e t}, \tag{30}$$

where $S_{\mathrm{FQM}}(t)$ and $R_{\mathrm{FQM}}(t)$ are given by

$$S_{\mathrm{FQM}}(t)=\mathbf{x}_1{}^T\mathcal{S}_{\mathrm{FQM}}\mathbf{x}_1\,, \tag{31}$$

and

$$R_{\mathrm{FQM}}(t)=\tfrac{1}{2}\,\mathrm{Tr}[\ln(\mathcal{R}_{\mathrm{FQM}}))-\ln(2\,\sinh(\beta\hbar\Omega_0/2))]. \tag{32}$$

In the above expressions we have also used the following notation:

$$\mathcal{R}_{\mathrm{FQM}}=\Omega_0^{-1}\,\sinh\{(\beta\hbar-it)\Omega_0\}\hbar^2(\mathcal{K}_0'+\mathcal{K}_1')\times(\mathcal{K}_0''+\mathcal{K}_1'')\Omega_1^{-1}\,\sinh(it\Omega_1), \tag{33}$$

$$\mathcal{S}_{\mathrm{FQM}}=\mathcal{K}_0'(\mathcal{K}_0'+\mathcal{K}_1')^{-1}\mathcal{K}_1', \tag{34}$$

$$\mathcal{K}_0'=\frac{1}{\hbar}\Omega_0\,\tanh\{(\beta-it/\hbar)\hbar\Omega_0/2\}, \tag{35}$$

$$\mathcal{K}_0''=\frac{1}{\hbar}\Omega_0\,\coth\{(\beta-it/\hbar)\hbar\Omega_0/2\}, \tag{36}$$

$$\mathcal{K}_1'=\frac{1}{\hbar}\Omega_1\,\tanh\{it\Omega_1/2\}, \tag{37}$$

$$\mathcal{K}_1''=\frac{1}{\hbar}\Omega_1\,\coth\{it\Omega_1/2\}. \tag{38}$$

Note that when the ''shift'' in the equilibrium position in the excited electronic state (relative to the ground state) vanishes, i.e., when $\mathbf{x}_1=\mathbf{0}$ ($\mathbf{x}_0$ was already set to zero), the function $S_{\mathrm{FQM}}(t)$ is identically equal to 0. Note also that when the coupling strength and the vibrational frequencies in the two electronic states are the same, i.e., when $g_\alpha^0=g_\alpha^1$ for all α, it can be shown[41] that the function $R_{\mathrm{FQM}}(t)$ is identically equal to 0. When the coupling strength in the two states is different, the two nuclear Hamiltonians H_0 and H_1 are characterized by different underlying sets of normal modes, i.e., there is a ''rotation'' involved in going from one set to the other. In view of the above, from now on we refer to $S_{\mathrm{FQM}}(t)$ as the ''shift'' term, and to $R_{\mathrm{FQM}}(t)$ as the ''rotation'' term in the dipole autocorrelation function.

To perform the calculation with the above equations, we have diagonalized the force constant matrices (Ω_0^2 and Ω_1^2) with the appropriate unitary transformations and evaluated functions of these matrices as follows:

$$f(M)=\mathcal{U}[f(\mathcal{U}^{-1}M\mathcal{U})]\mathcal{U}^{-1}, \tag{39}$$

where M is a matrix, f is an analytic function and $\mathcal{U}^{-1}M\mathcal{U}$ is a diagonal matrix, so that the function f of the latter can be easily obtained.

B. The dynamic and static classical limits of $C(t)$

In this subsection we adopt a semiclassical approach, where the two electronic states are treated quantum mechanically, while all nuclear degrees of freedom are treated classically (either dynamically or statically).[14,16,34,43,45] For the dynamic limit we use two propagation schemes.

The first (DCL) is based on the time-ordered exponential (Eq. (16)), which in the classical limit takes the form

$$C_{\mathrm{DCL}}(t)=\left\langle \exp\left\{-\frac{i}{\hbar}\int_0^t dt'\,\Delta(t')\right\}\right\rangle_{cl}, \tag{40}$$

where $\langle\cdots\rangle_{cl}$ denotes a classical equilibrium ensemble average over initial coordinates and momenta weighted by the Boltzmann factor for the ground state nuclear Hamiltonian. In contrast to Eq. (16), there is no time ordering, and $\Delta(t)$ is no longer a Heisenberg operator, but rather a function of *dynamic* classical variables, whose time dependence is governed by the ground state nuclear Hamiltonian, as is clear from Eq. (17).

The second propagation scheme (ACL) can be obtained by expanding $\mathcal{L}$ in Eq. (21) in powers of $\hbar$ and retaining only the terms of order $\hbar^{-1}$ and $\hbar^0$. For this approximation, $C(t)$ from Eq. (19) takes the simpler form[16]

$$C_{\mathrm{ACL}}(t)=\left\langle \exp\left\{-\frac{i}{\hbar}\int_0^t dt'\,\Delta_{\mathrm{av}}(t')\right\}\right\rangle_{cl}, \tag{41}$$

where $\Delta_{\mathrm{av}}(t)$ is the difference between the excited and ground state Hamiltonians propagated under the arithmetic average of the two Hamiltonians (and averaged over the ground state equilibrium distribution):[16]

$$\Delta_{\mathrm{av}}(t)=e^{i(H_0+H_1)t/(2\hbar)}\Delta e^{-i(H_0+H_1)t/(2\hbar)}. \tag{42}$$

Note that Eq. (41) can also be obtained from the time-ordered exponential similarly to Eq. (40) by using the interaction picture governed by the averaged Hamiltonian (Eq. (42)) instead of the ground state one.

In order to obtain the time dependence of $\Delta(t)$ ($\Delta_{\mathrm{av}}(t)$) for the two propagation schemes one needs to diagonalize the ground state force constant matrix Ω_0^2 (or the arithmetic average $(\Omega_0^2+\Omega_1^2)/2)$) with the appropriate unitary transformation. For the current problem, the remaining classical equilibrium average in both cases can be performed analytically to obtain $C(t)$. However, we will present only the derivation of the DCL of $C(t)$, since the derivation of the ACL follows exactly the same lines.

In view of the above discussion, we start by diagonalizing the ground state force constant matrix with the appropriate unitary transformation $\mathcal{U}_0$,

$$\tilde{\Omega}_0^2=\mathcal{U}_0^T\Omega_0^2\mathcal{U}_0, \tag{43}$$

where $\tilde{\Omega}_0^2$ is a diagonal matrix with N_b+1 elements $\tilde{\omega}_j^2$ which are the squares of the frequencies of the ground state normal modes. The excited state force constant matrix transformed under $\mathcal{U}_0$ becomes

$$\tilde{\Omega}_1^2=\mathcal{U}_0^T\Omega_1^2\mathcal{U}_0, \tag{44}$$

and in general is not diagonal except for the case of the same coupling strength for both electronic states. For future purposes we introduce a matrix

$$\tilde{\Omega}^2=\mathcal{U}_0^T(\Omega_1^2-\Omega_0^2)\mathcal{U}_0. \tag{45}$$

For the present problem, the time integral in Eq. (40) can be performed analytically once $\Delta(t)$ is expressed in terms of the ground state normal modes, whose time dependence is particularly simple

$$\tilde{q}_j(t)=\tilde{q}_j(0)\cos(\tilde{\omega}_j t)+\frac{\tilde{p}_j(0)}{\tilde{\omega}_j}\sin(\tilde{\omega}_j t), \tag{46}$$

where $\tilde{q}_j(0)$ and $\tilde{p}_j(0)$ are the initial position and momentum of normal mode j, respectively. The classical equilibrium average then reduces to Gaussian integrals over initial coordinates and momenta (note that $\Delta(t)$ depends on the initial positions as well as on the initial momenta through the time dependence of the normal modes). Expressing $\mathbf{x}$ in terms of the ground state normal modes and performing the integrals, yields the following result for the dynamical classical limit of $C(t)$:

$$C_{\mathrm{DCL}}(t)=e^{-S_{\mathrm{DCL}}(t)}e^{-R_{\mathrm{DCL}}(t)}e^{-i\omega_e t}, \tag{47}$$

where (recall that $\mathbf{x}_0=\mathbf{0}$)

$$S_{\mathrm{DCL}}(t)=\frac{1}{2\hbar}(\xi^T\mathcal{S}_{\mathrm{DCL}}\xi+i\mathbf{x}_1^T\Omega_1^2\mathbf{x}_1 t), \tag{48}$$

and

$$R_{\mathrm{DCL}}(t)=-\tfrac{1}{2}\mathrm{Tr}[\ln(\mathcal{R}_{\mathrm{DCL}}))-\ln(\beta\hbar\Omega_0)]. \tag{49}$$

$\mathcal{S}_{\mathrm{DCL}}$ and $\mathcal{R}_{\mathrm{DCL}}$ are square matrices of rank $2N=2N_b+2$ and $\mathcal{S}_{\mathrm{DCL}}=\mathcal{R}_{DCL}^{-1}$. In what follows, the indices j and k run from 1 to N. The vector ξ of length $2N$ has the following elements:

$$\xi_j=[\mathbf{x}_1^T\Omega_1^2\mathcal{U}_0]_j\,\sin(\tilde{\omega}_j t)/\tilde{\omega}_j^{3/2}, \tag{50}$$

and

$$\xi_{j+N}=[\mathbf{x}_1^T\Omega_1^2\mathcal{U}_0]_j(1-\cos(\tilde{\omega}_j t))/\tilde{\omega}_j^{3/2}. \tag{51}$$

The matrix elements of $\mathcal{R}_{\mathrm{DCL}}$ are in the form

$$[\mathcal{R}_{\mathrm{DCL}}]_{j,k}=\frac{i}{2}\,\tilde{\Omega}_{jk}^2F_{j,k}(t)+\beta\hbar\tilde{\omega}_j\delta_{jk}, \tag{52}$$

$$[\mathcal{R}_{\mathrm{DCL}}]_{j+N,k}=\frac{i}{2}\,\tilde{\Omega}_{jk}^2F_{j+N,k}(t), \tag{53}$$

$$[\mathcal{R}_{\mathrm{DCL}}]_{j,k+N}=\frac{i}{2}\,\tilde{\Omega}_{jk}^2F_{j,k+N}(t), \tag{54}$$

$$[\mathcal{R}_{\mathrm{DCL}}]_{j+N,k+N}=\frac{i}{2}\,\tilde{\Omega}_{jk}^2F_{j+N,k+N}(t)+\beta\hbar\tilde{\omega}_j\delta_{jk}, \tag{55}$$

where δ_{jk} is the Kronecker delta symbol. In the above expressions we have also used the following notation:

$$F_{j,k}=\frac{\sin[(\tilde{\omega}_j-\tilde{\omega}_k)t]}{(\tilde{\omega}_j-\tilde{\omega}_k)\sqrt{\tilde{\omega}_j\tilde{\omega}_k}}+\frac{\sin[(\tilde{\omega}_j+\tilde{\omega}_k)t]}{(\tilde{\omega}_j+\tilde{\omega}_k)\sqrt{\tilde{\omega}_j\tilde{\omega}_k}}, \tag{56}$$

$$F_{j+N,k}=\frac{1-\cos[(\tilde{\omega}_j-\tilde{\omega}_k)t]}{(\tilde{\omega}_j-\tilde{\omega}_k)\sqrt{\tilde{\omega}_j\tilde{\omega}_k}}+\frac{1-\cos[(\tilde{\omega}_j+\tilde{\omega}_k)t]}{(\tilde{\omega}_j+\tilde{\omega}_k)\sqrt{\tilde{\omega}_j\tilde{\omega}_k}}, \tag{57}$$

$$F_{j,k+N}=\frac{1-\cos[(\tilde{\omega}_k-\tilde{\omega}_j)t]}{(\tilde{\omega}_k-\tilde{\omega}_j)\sqrt{\tilde{\omega}_j\tilde{\omega}_k}}+\frac{1-\cos[(\tilde{\omega}_k+\tilde{\omega}_j)t]}{(\tilde{\omega}_k+\tilde{\omega}_j)\sqrt{\tilde{\omega}_j\tilde{\omega}_k}}, \tag{58}$$

$$F_{j+N,k+N}=\frac{\sin[(\tilde{\omega}_j-\tilde{\omega}_k)t]}{(\tilde{\omega}_j-\tilde{\omega}_k)\sqrt{\tilde{\omega}_j\tilde{\omega}_k}}-\frac{\sin[(\tilde{\omega}_j+\tilde{\omega}_k)t]}{(\tilde{\omega}_j+\tilde{\omega}_k)\sqrt{\tilde{\omega}_j\tilde{\omega}_k}}. \tag{59}$$

In the case $\tilde{\omega}_j=\tilde{\omega}_k$ the appropriate limit of the above must be taken.

The above derivation (along with the extension to ACL) is one of the central results in this paper, since the DCL is widely used to estimate the vibronic absorption spectrum in systems where the FQM treatment is still not feasible.[17,18] Therefore, the above derivation of the absorption spectrum provides a direct tool to investigate the validity of the DCL approximation for the present problem. At the same time, we are also able to assess the accuracy of the average dynamical limit, and below we will discuss the differences between the two semiclassical approximations.

Before we proceed to discuss the MQC case, we briefly outline the results for the SCL, which is of interest for inhomogeneously broadened spectra. One can obtain the $C_{\mathrm{SCL}}(t)$ by freezing all nuclear degrees of freedom,[41,43,46] in which case Eq. (16) takes the simpler form

$$C_{\mathrm{SCL}}(t)=\left\langle \exp\left\{-\frac{it}{\hbar}\Delta\right\}\right\rangle_{cl}, \tag{60}$$

where Δ is given by Eq. (18). Performing the Gaussian integrals over coordinates and momenta yields the desired SCL result. However, a simpler way to obtain $C_{\mathrm{SCL}}(t)$ is to take the short time limit of $S_{\mathrm{DCL}}(t)$ and $R_{\mathrm{DCL}}(t)$ in Eq. (47).

C. The mixed quantum-classical limit of $C(t)$

An alternative expression for the real-time dipole correlation function for the fully quantum mechanical system can be derived using path integrals. After integrating out the harmonic bath degrees of freedom,[44,47] $C(t)$ can be expressed in terms of the molecular system propagator and in terms of the influence functional representing the environment:

$$C(t)=\int \mathcal{D}q\mathcal{D}q^+\mathcal{D}q^-\ \exp\left\{-\beta h_0(q)+\frac{i}{\hbar}(S_0[q^+]-S_1[q^-])\right\}I(q^+,q^-,q,t)/Z(\beta), \tag{61}$$

where $I(q^+,q^-,q,t)$ is the influence functional of the bath, and q^+, q^- and q are the forward, backward and thermal path, respectively. In the above, $h_0(q)$ is the ground state vibrational Hamiltonian (Eq. (4)) and $Z(\beta)$ is the partition function (Eq. (15)). The classical actions, $S_0[q]$ and $S_1[q]$, for the diatomic vibrational mode for state $|0\rangle$, or state $|1\rangle$, respectively, are given by

$$S_{0,1}[q]=\frac{1}{2}\int_0^t dt'[\dot{q}^2-\omega_{0,1}^2(q-q_{0,1})^2]. \tag{62}$$

A general expression for $I(q^+,q^-,q,t)$ for the present problem can be obtained after a straightforward but tedious calculation; the result is given in the Appendix. For reasons which will become clear below, the MQC treatment will be applied to the case of zero diatomic-bath coupling in the ground electronic state. In this case the influence functional takes a simpler form

$$I(q^+,q^-,q,t) = \exp\left\{ -\frac{1}{\hbar^2}\int_0^t dt_1 \int_0^{t_1} dt_2 q^-(t_1)q^-(t_2) \times \sum_{\alpha}^{N_b} (g_\alpha^1)^2 \chi_\alpha(t_1-t_2) \right\}, \tag{63}$$

which depends only on the backwards path (q^-). In the above $\chi_\alpha(t_1-t_2)=\langle Q_\alpha(t_1)Q_\alpha(t_2)\rangle$ is the real-time bath position autocorrelation function

$$\chi_\alpha(t_1-t_2)=\frac{\hbar}{2\omega_\alpha}\{\coth[\beta\hbar\omega_\alpha/2]\cos(\omega_\alpha(t_1-t_2)) - i\,\sin(\omega_\alpha(t_1-t_2))\}. \tag{64}$$

Next we use the short time Trotter formula[48,49] for the diatomic propagator that appears in Eq. (61) and replace the q-dependent potential terms (including the terms in the influence functional) with a trapezoidal approximation. We then split the time integrals in the influence functional in accordance with the Trotter factorization of the diatomic path. Next we perform the integration over the time variables in the influence functional for each time slice, keeping the value of the diatomic coordinate fixed (this requires a sufficiently small time step). This procedure is better than assuming in addition a constant value for the autocorrelation function itself, since the bath might have higher frequency modes than the diatomic vibration. The remaining integrals over the sliced diatomic path become simple Gaussian integrals, which we perform analytically. This procedure is by no means unique, and can readily be improved by using more sophisticated factorization schemes.[50] However, for the present purposes we found that a simple Trotter split is sufficient, and can reproduce with good accuracy the FQM results obtained using Eq. (30).

In the present formulation, it is straightforward to take the dynamical classical limit for the bath modes, keeping the quantum description of the diatomic vibrational coordinate. In order to do this, one simply replaces the quantum bath correlation function by its classical analogue

$$\chi_\alpha^{cl}(t_1-t_2)=\frac{1}{\beta\omega_\alpha^2}\cos(\omega_\alpha(t_1-t_2)). \tag{65}$$

Inserting $\chi_\alpha^{cl}(t)$ in the influence functional and following the procedure outlined above yields the MQC limit for the dipole autocorrelation function $C_{\mathrm{MQC}}(t)$. Unlike the fully quantum mechanical derivation, the present MQC approximation is not limited to a finite number of bath modes. However, it is limited to shorter times than FQM, due to the time slicing (as mentioned above, for the present problem this limitation of the MQC does not appear in the results for the absorption spectra). We have also used and alternative approach to derive the MQC limit by judiciously neglecting appropriate (bath) commutators and replacing the trace over the bath modes with the classical integral over phase space in Eq. (13).

IV. ASYMPTOTIC LONG TIME BEHAVIOR OF THE DIPOLE AUTOCORRELATION FUNCTION

In this section we present the analytic results for the asymptotic long time behavior of the FQM, DCL, ACL and MQC of $C(t)$. Our treatment is based on the non-perturbative theory of Hsu and Skinner,[34,35] who have obtained the corresponding asymptotic results for a problem involving two completely general harmonic potential energy surfaces (i.e., including the possibility of equilibrium position displacements, frequency shifts and mode mixing) using a cumulant expansion of the time-ordered exponential in Eq. (16). As such, their results are directly applicable to the problem at hand. The (fully quantum mechanical) derivation of Hsu and Skinner assumes the factorization of the initial density operator into a product of the electronic two-level system density operator and the equilibrium bath density operator. Since we are concerned here with the asymptotic long time behavior of the dipole autocorrelation functions, the above approximation should not affect the results; we will assess its accuracy by comparing the analytic asymptotic results obtained below with the exact results for the time correlation functions presented in the previous Section.

Guided by the work of Hsu and Skinner for a somewhat different Hamiltonian,[35] it can be shown that for times much longer than the characteristic decay time of the bath fluctuations, the time dependence of the $C_{\mathrm{FQM}}(t)$ takes the following asymptotic form:

$$C_{\mathrm{FQM}}(t)\propto e^{-i\omega_e t}e^{-\eta t}, \tag{66}$$

where

$$\eta=\frac{i}{2\hbar}\mathbf{x}_1^T\Omega_1^2U_0\Lambda(0)(1-\tilde{\Omega}^2\Lambda(0))^{-1}U_0^T\Omega_1^2\mathbf{x}_1 + \frac{i}{2\hbar}\mathbf{x}_1^T\Omega_1^2\mathbf{x}_1+\frac{1}{2\pi}\int_0^\infty d\omega \times \ln(\det[E+i\tilde{\Omega}^2\{(2n(\omega)+1)\Gamma(\omega)+i\Lambda(\omega)\}]). \tag{67}$$

The second term in Eq. (67) is absent from Eq. (26) of Reference 35, since their nuclear Hamiltonian for the excited electronic state differs from our definition of H_1 by the constant term $\frac{1}{2}\mathbf{x}_1^T\Omega_1^2\mathbf{x}_1$. In the above $n(\omega)=(\exp(\beta\hbar\omega)-1)^{-1}$ is the phonon thermal occupation number, E is a unity matrix of rank N, $\Gamma(\omega)$ is the weighted density of states matrix of rank N defined according to[35]

$$[\Gamma(\omega)]_{jk}=\frac{\pi}{2\tilde{\omega}_j}\delta(\omega-\tilde{\omega}_j)\delta_{jk}, \tag{68}$$

and $\Lambda(\omega)$ is the following $N\times N$ matrix:

$$\Lambda(\omega)=\frac{2}{\pi}P\int_0^\infty d\omega'\Gamma(\omega')\left(\frac{\omega'}{\omega^2-\omega'^2}\right), \tag{69}$$

where P stands for the principal value of the integral. For future use, we note the following relation:[35]

$$\Lambda(0) = -\frac{2}{\pi}\int_0^\infty d\omega \Gamma(\omega)/\omega. \tag{70}$$

To make connection with spectroscopic quantities, we rewrite Eq. (66) in the following form:

$$C_{\mathrm{FQM}}(t) \propto e^{-i(\Delta\omega_{\mathrm{FQM}}+\omega_e)t} e^{-t/T_2^{\mathrm{FQM}}}, \tag{71}$$

where $1/T_2^{\mathrm{FQM}} = \mathrm{Re}[\eta]$ is the dephasing rate and $\Delta\omega_{\mathrm{FQM}} = \mathrm{Im}[\eta]$ is the frequency shift. Finding the real and imaginary parts of η yields the following expressions for the dephasing rate:

$$\frac{1}{T_2^{\mathrm{FQM}}} = \frac{1}{4\pi}\int_0^\infty d\omega \ \ln\{\det[(1-\tilde{\Omega}^2\Lambda(\omega))^2 + (2n(\omega)+1)^2(\tilde{\Omega}^2\Gamma(\omega))^2]\}, \tag{72}$$

and for the frequency shift

$$\Delta\omega_{\mathrm{FQM}} = \frac{1}{2\hbar}\mathbf{x}_1^T\Omega_1^2 U_0\Lambda(0)(1-\tilde{\Omega}^2\Lambda(0))^{-1}U_0^T\Omega_1^2\mathbf{x}_1 + \frac{1}{2\hbar}\mathbf{x}_1^T\Omega_1^2\mathbf{x}_1 + \frac{1}{2\pi}\int_0^\infty d\omega \mathrm{Tr}[\arctan((2n(\omega)+1)(1-\tilde{\Omega}^2\Lambda(\omega))^{-1}\tilde{\Omega}^2)]. \tag{73}$$

Using Eq. (70) one can easily show that the first two terms in Eq. (73) exactly cancel each other, and the result for the frequency shift simplifies considerably

$$\Delta\omega_{\mathrm{FQM}} = \frac{1}{2\pi}\int_0^\infty d\omega \mathrm{Tr}[\arctan((2n(\omega)+1) \times (1-\tilde{\Omega}^2\Lambda(\omega))^{-1}\tilde{\Omega}^2\Gamma(\omega))]. \tag{74}$$

From the above it is clear that both the dephasing rate $1/T_2^{\mathrm{FQM}}$ and the frequency shift $\Delta\omega_{\mathrm{FQM}}$ are independent of the relative ‘‘shift’’ in the equilibrium position $\mathbf{x}_1$, and depend only on the ‘‘rotation’’ of the normal modes in the excited state relative to the ground state, i.e., on the difference in the coupling strength. Therefore, in the long time limit one can identify the slopes of the real and imaginary parts of $R_{\mathrm{FQM}}(t)$ with the dephasing rate and frequency shift, respectively,

$$\mathrm{Re}[R_{\mathrm{FQM}}(t)] = c_{re} + t/T_2^{\mathrm{FQM}}, \tag{75}$$

and

$$\mathrm{Im}[R_{\mathrm{FQM}}(t)] = c_{im} + t\Delta\omega_{\mathrm{FQM}}, \tag{76}$$

where c_{re} and c_{im} are two unknown constants.

We now proceed to discuss the asymptotic long time behavior of $C_{\mathrm{DCL}}(t)$, which is qualitatively similar[34,45] to $C_{\mathrm{FQM}}(t)$,

$$C_{\mathrm{DCL}}(t) \propto e^{-i(\Delta\omega_{\mathrm{DCL}}+\omega_e)t} e^{-t/T_2^{\mathrm{DCL}}}. \tag{77}$$

As pointed out by Skinner and Hsu,[34] the dephasing rate and the frequency shift in the semiclassical limit can be obtained from the FQM results by setting the matrix $\Lambda(\omega)$ equal to 0. In addition, one needs to replace the expression $(2n(\omega)+1)$ by its high temperature limit $2/\beta\hbar\omega$. Applying this procedure to Eq. (72) yields for the DCL dephasing rate

$$\frac{1}{T_2^{\mathrm{DCL}}} = \frac{1}{4\pi}\int_0^\infty d\omega \ \ln\{\det[1+(2/\beta\hbar\omega)^2(\tilde{\Omega}^2\Gamma(\omega))^2]\}, \tag{78}$$

and using the same procedure in Eq. (73) gives for the DCL frequency shift

$$\Delta\omega_{\mathrm{DCL}} = \frac{1}{2\hbar}\mathbf{x}_1^T\Omega_1^2\mathbf{x}_1 + \frac{1}{2\pi}\int_0^\infty d\omega \times \mathrm{Tr}[\arctan((2/\beta\hbar\omega)\tilde{\Omega}^2\Gamma(\omega))]. \tag{79}$$

Note that $\Delta\omega_{\mathrm{DCL}}$ contains a term which depends on the ‘‘shift’’ in the equilibrium position $\mathbf{x}_1$ since the first term in Eq. (73) (which served to cancel the above term in the FQM case) is proportional to $\Lambda(0)$ and therefore vanishes in the dynamical classical limit.

Thus, in the dynamic classical limit (in contrast to the FQM case) the frequency shift $\Delta\omega_{\mathrm{DCL}}$ depends both on the relative ‘‘shift’’ in the equilibrium position $\mathbf{x}_1$, and on the ‘‘rotation’’ of the normal modes in the excited state relative to the ground state. In the long time limit, the slope of the imaginary part of $S_{\mathrm{DCL}}(t)$ can be identified with the first term in Eq. (79), and the imaginary part of $R_{\mathrm{DCL}}(t)$ can be identified with the second term in this equation. At the same time, the dephasing rate $1/T_2^{\mathrm{DCL}}$ depends only on the ‘‘rotation’’ of the normal modes in the excited state relative to the ground state. Therefore, in the long time limit one can identify the slope of the real part of $R_{\mathrm{DCL}}(t)$ with the dephasing rate. Hence, in the long time limit we have

$$\mathrm{Re}[R_{\mathrm{DCL}}(t)] = c'_{re} + t/T_2^{\mathrm{DCL}}, \tag{80}$$

$$\mathrm{Im}[R_{\mathrm{DCL}}(t)] = c'_{im} + t\Delta\omega_{\mathrm{DCL}} - \frac{t}{2\hbar}\mathbf{x}_1^T\Omega_1^2\mathbf{x}_1, \tag{81}$$

and

$$\mathrm{Im}[S_{\mathrm{DCL}}(t)] = c''_{im} + \frac{t}{2\hbar}\mathbf{x}_1^T\Omega_1^2\mathbf{x}_1. \tag{82}$$

The derivation of the long time asymptotic behavior of $C_{\mathrm{ACL}}(t)$ is analogous to the DCL case. Analysis of the cumulant expansion[34] of Eq. (41) shows that for the purpose of calculating the long time asymptotic behavior of $C_{\mathrm{ACL}}(t)$, the classical thermal averaging over the *ground* state Hamiltonian in Eq. (41) can be replaced by the classical thermal averaging on the *averaged* Hamiltonian (cf. Eq. (23)). Although not entirely justified, it is often assumed that the behavior at long times should not depend on the initial preparation of the system. We therefore replace the ground state normal mode frequencies $(\tilde{\omega}_j)$ with the averaged Hamiltonian normal mode frequencies $(\tilde{\omega}_j^{\mathrm{av}})$. The weighted density of state in Eq. (68) then takes the form

$$[\Gamma_{\mathrm{av}}(\omega)]_{jk}=\frac{\pi}{2\tilde{\omega}_j^{\mathrm{av}}}\,\delta(\omega-\tilde{\omega}_j^{\mathrm{av}})\,\delta_{jk}. \tag{83}$$

In addition, in calculating the matrix $\tilde{\Omega}^2$ from Eq. (45), we replace the unitary transformation $\mathcal{U}_0$ with the appropriate unitary transformation ($\mathcal{U}_{\mathrm{av}}$) which diagonalizes the averaged Hamiltonian

$$\tilde{\Omega}_{\mathrm{av}}^2=\mathcal{U}_{\mathrm{av}}^T(\Omega_1^2-\Omega_0^2)\mathcal{U}_{\mathrm{av}}. \tag{84}$$

This yields the following result for the ACL dephasing rate:

$$\frac{1}{T_2^{\mathrm{ACL}}}=\frac{1}{4\pi}\int_0^\infty d\omega\,\ln\{\det[1+(2/\beta\hbar\omega)^2 \times(\tilde{\Omega}_{\mathrm{av}}^2\Gamma_{\mathrm{av}}(\omega))^2]\}, \tag{85}$$

and for the ACL frequency shift

$$\Delta\omega_{\mathrm{ACL}}=\frac{1}{8\hbar}\mathbf{x}_1^T(\Omega_1^2-\Omega_0^2)\mathbf{x}_1+\frac{1}{2\pi}\int_0^\infty d\omega \times\mathrm{Tr}[\arctan((2/\beta\hbar\omega)\tilde{\Omega}_{\mathrm{av}}^2\Gamma_{\mathrm{av}}(\omega))]. \tag{86}$$

Note that $\Delta\omega_{\mathrm{ACL}}$ contains a term which depends on the "shift" in the equilibrium position $\mathbf{x}_1$. However, this term is different from the DCL term in Eq. (79), and vanishes for the case of the same vibrational frequencies in both electronic states.

The discussion of the asymptotic long time behavior of $C_{\mathrm{MQC}}(t)$ will be limited to the case when the coupling strength in the ground electronic state is zero ($\rho_0=0$). In this simpler case, the nuclear coordinates in the original ("untransformed") ground electronic state Hamiltonian form a set of normal modes. Therefore the (diagonal) matrices $\Gamma(\omega)$ and $\Lambda(\omega)$ can be immediately expressed in terms of N_b bath modes and the diatomic vibrational coordinate. Since we would like to treat the former classically and the latter quantum mechanically, we set all elements of $\Lambda(\omega)$ which correspond to the bath modes equal to zero, and retain only the element corresponding to the diatomic mode. Inserting this "truncated" matrix $\Lambda(\omega)$ into Eqs. (72) and (73), and replacing $(2n(\omega)+1)$ by $2/\beta\hbar\omega$, yields the results for the dephasing rate and the frequency shift in the MQC limit. Since the form of the equations is identical to the FQM case, we do not reproduce them here, but rather provide numerical results in the following section.

In the next section we test the accuracy of the quantum mechanical, dynamical classical and mixed quantum-classical results for the frequency shift and the dephasing rate by calculating the dipole autocorrelation function exactly at all times (using the results of Section III) and by comparing its asymptotic long time behavior with the theoretical predictions from the present Section.

V. RESULTS AND DISCUSSION

We perform exact calculations of the dipole autocorrelation functions for the fully quantum mechanical treatment and for all its semiclassical limits. As mentioned earlier, the numerical calculations are limited to a finite number N_b of bath modes. In order to obtain the coupling coefficients which would mimic the appropriate continuous spectral density, the following procedure[51] was utilized: $J_{0,1}(\omega)$ was discretized evenly with an increment $\delta\omega$, and the coupling coefficients were calculated according to

$$(g_\alpha^{0,1})^2=2\omega_\alpha J_{0,1}(\omega_\alpha)\delta\omega. \tag{87}$$

The bath spectral density, $J_{0,1}(\omega_\alpha)$ is given by Eq. (9). In all calculations shown below we choose the cutoff parameter (from now on we employ atomic units) $\gamma=5$. In performing the calculations, we have checked for the convergence with respect to the number of modes by increasing N_b until no further change in the Fourier transforms of the calculated correlation functions (i.e., absorption spectra) was observed. Typically, $N_b=30$ was found to be sufficient to achieve convergence, however, the results reported below were obtained setting $N_b=100$.

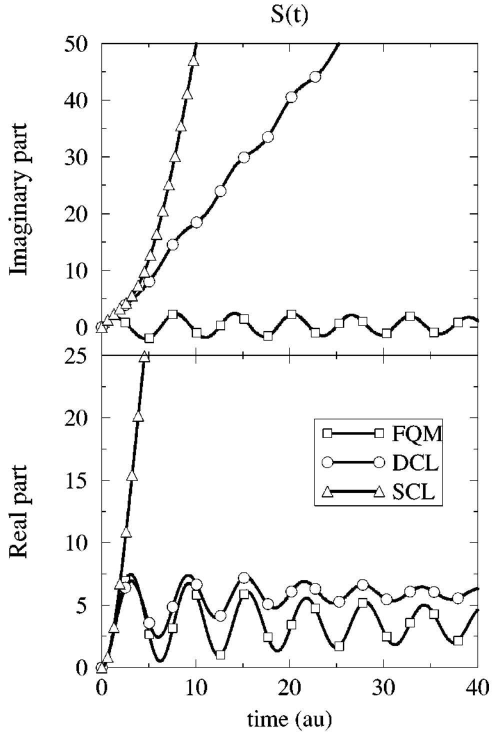

FIG. 1. Plots of the real and imaginary parts of the "shift" function $S(t)$ vs time for $\beta=1$, $\rho_0=0.0625$ and $\rho_1=0.025$. The vibrational frequency of the diatomic molecule is set to unity and the "shift" in the equilibrium position of the diatomic is $q_1=2$. The squares, circles and triangles are the results of the FQM, DCL and SCL cases, respectively. Note the good agreement at short times between all three curves, while for intermediate times there are discrepancies.

The first set of calculations is performed for the inverse temperature $\beta=1$ with the following values of the ground and excited state coupling parameters: $q_0=0$, $q_1=2$, $\omega_0=\omega_1=1$, $\rho_0=0.0625$ and $\rho_1=0.025$; we set $\omega_e=0$. The results for real and imaginary parts of the "shift" functions $S(t)$ for FQM, DCL and SCL (at short and intermediate times) are shown in Fig. 1. In Fig 2 we plot the results for the real and imaginary parts of the "rotation" functions $R(t)$ for the three cases (again at short and intermediate times).

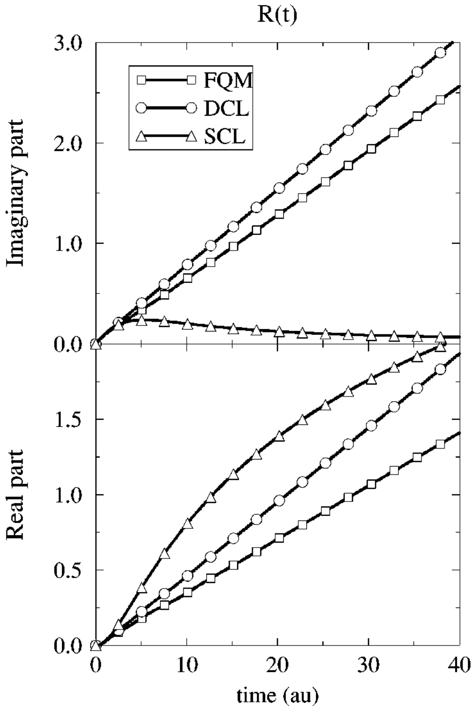

FIG. 2. Plots of the real and imaginary parts of the ''rotation'' function $R(t)$ vs time. The parameters are the same as in Fig. 1. The real and imaginary parts of $R(t)$ for the FQM and DCL approach the linear regime at relatively short times, while the SCL displays a non-linear dependence over the time range shown.

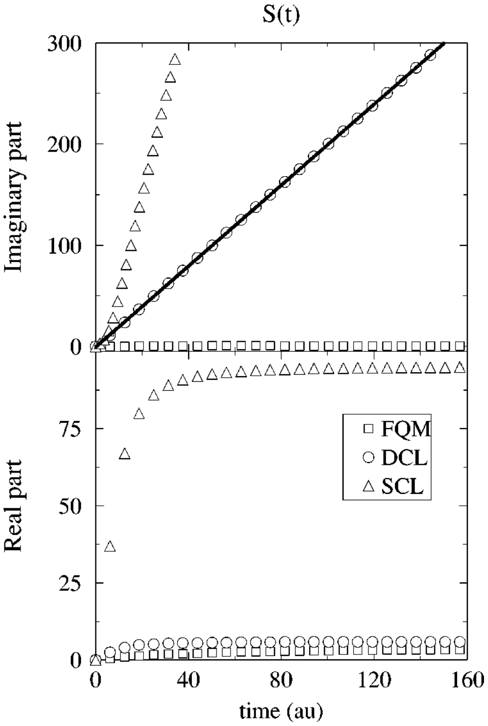

FIG. 3. Plots of the asymptotic long time behavior of the ''shift'' function $S(t)$ for the same set of parameters as in Fig. 1. The real parts of all three function tend to (different) constant values at long times. The behavior of the imaginary part is somewhat different: while $S_{\mathrm{FQM}}(t)$ tends to a constant value at long times, $S_{\mathrm{DCL}}(t)$ increases linearly with time and $S_{\mathrm{SCL}}(t)$ increases even faster. The solid line is the theoretical long time DCL result (cf. the first term of Eq. (82)).

At very short times, all three results agree very closely with each other. This is not surprising, since the classical treatment of the dynamics is known to be accurate for short times. Moreover, as mentioned above, in the short time limit the DCL result reduces to the SCL. We have also calculated the first two moments of the spectral line shape and obtained excellent agreement between the three cases. This is consistent with the result obtained by Lax.[43] At longer times the SCL result deviates markedly from the other two (FQM and DCL) cases. In particular the real part of $S_{\mathrm{SCL}}(t)$ does not have any oscillations which implies that the SCL spectrum is structureless, as one would expect from the *classical* Franck–Condon treatment.

We now turn to the asymptotic long time behavior of the ''shift'' and ''rotation'' functions. Regarding the FQM result, we observe that both real and imaginary parts of the ''shift'' function $S_{\mathrm{FQM}}(t)$ eventually tend to a constant value, whereas both real and imaginary parts of the ''rotation'' quantum function $R_{\mathrm{FQM}}(t)$ depend linearly on time at long times. This is consistent with the results of the previous section (Eqs. (75) and (76)).

The long time behavior of the dynamical classical ''rotation'' function $R_{\mathrm{DCL}}(t)$ is qualitatively similar to its quantum counterpart, albeit the slopes have different numerical values, as follows from the equations for frequency shift $\Delta\omega_{\mathrm{DCL}}$ (Eq. (79)) and the dephasing rate $1/T_2^{\mathrm{DCL}}$ (Eq. (78)). Regarding the ''shift'' function $S_{\mathrm{DCL}}(t)$, we observe that at long times its real part tends to a constant, whereas the imaginary part displays a linear time dependence. This is consistent with the results of the previous section (Eqs. (80), (81) and (82)).

In Figs. 3 and 4 we show the asymptotic long time behavior of the ''shift'' and ''rotation'' functions (symbols) along with the theoretical (lines) asymptotic long time results (Eqs. (75), (76), (80), (81) and (82)). We adjust the unknown intercepts of each linear functions to obtain an agreement at long time, however the slopes are taken directly from theory and are not adjusted. As is clearly seen in the figures the present asymptotic long time theoretical results agree with the exact numerical calculations at long times.

We would like to point out that, as expected, the long time behavior of the dipole autocorrelation function in the SCL is qualitatively different from the two cases discussed above. In particular, at long times the real and imaginary parts of $R_{\mathrm{SCL}}(t)$ and $S_{\mathrm{SCL}}(t)$ are not linear functions of time. In the frequency domain this implies a non-Lorentzian spectral line shape.

Finally, we have performed the same calculations for ACL (at all times), but do not present them here, since they are essentially indistinguishable from the FQM results, for the above parameters. We note that the ACL theoretical asymptotic long time behavior given in Eqs. (85) and (86) is in excellent agreement with the exact numerical calculations at long time.

We have calculated the dipole autocorrelation functions for several other sets of parameters (β, ρ_0 and ρ_1), the results

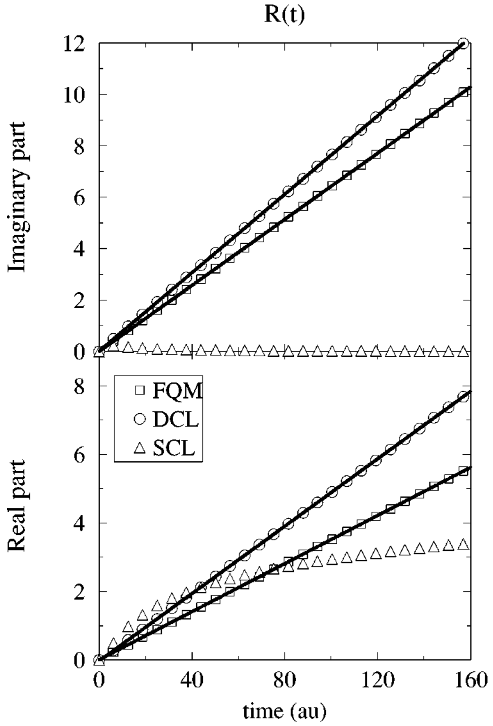

FIG. 4. Plots of the asymptotic long time behavior of the ''rotation'' function $R(t)$ for the same set of parameters as in Fig. 1. The expected linear long time behavior of the $R_{\mathrm{DCL}}(t)$ is qualitatively similar to $R_{\mathrm{FQM}}(t)$, but the slopes have different numerical values. The solid curves are the theoretical long time results based on Eqs. (75), (76), (80) and (81). The long time behavior of the ''rotation'' function in the static classical limit, $R_{\mathrm{SCL}}(t)$, is quite different and does not change linearly with time.

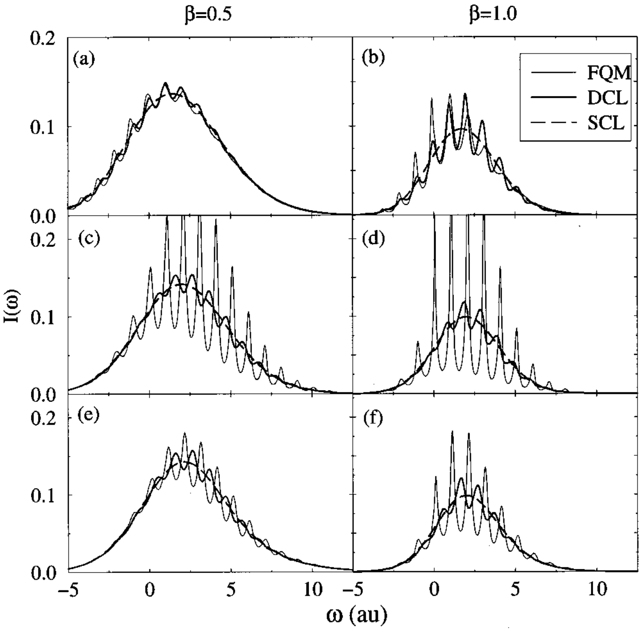

FIG. 5. Plots of the electronic absorption spectrum of a diatomic molecule coupled to a harmonic bath for two different temperatures ($\beta=0.5$ and $\beta=1$). The thin solid, thick solid and dashed lines are for FQM, DCL and SCL results, respectively. In order to have the same vertical scale for all panels, we normalized the high temperature spectra to unity, whereas the lower temperature spectra were normalized to half. The top ((a) and (b)), middle ((c) and (d)), and bottom ((e) and (f)) rows are for coupling strength ρ_0 and ρ_1 of 0.05 and 0.125, 0.0625 and 0.025, 0.125 and 0.05, respectively. The vibrational frequencies ω_0 and ω_1 are set equal to unity. The SCL absorption spectrum is structureless, whereas both FQM and DCL results are characterized by a vibronic structure. As expected, the agreement between FQM and DCL is better at higher temperatures.

obtained are similar to the ones presented in Figs. 1–4, and we do not show them here.

We now proceed to discuss the absorption spectra given by the Fourier transforms of the dipole autocorrelation functions (Eq. (10)). We have calculated $I(\omega)$ for two values of the inverse temperature ($\beta=0.5$ and $\beta=1$), and for each of these values of β-for three sets of coupling strengths (see figure caption). The results are plotted in Fig. 5, for vibrational frequencies of $\omega_0=\omega_1=1$. As already discussed earlier, the SCL spectrum (dashed line) is structureless, whereas both the FQM and the DCL spectra, $I(\omega)$, are characterized by fine vibronic structure superimposed on a wide absorption band. The SCL result reproduces well the center position and the width of this wide band, since the first two moments are essentially exact in the classical limit.

While the DCL spectrum certainly represents an improvement over the SCL result, it is not in quantitative agreement with the FQM spectrum. The widths of individual vibronic features are overestimated in the dynamical classical treatment. This discrepancy between the two is larger than what would be expected on the basis of comparing the dephasing rates. Presumably, additional broadening arises in the DCL due to a faster decay (at intermediate times) of the ''shift'' term in the dipole autocorrelation function. Concomitantly, the amplitudes of vibronic features are different in the two treatments, because both spectra are normalized in the same way. It seems that when the coupling strength is larger for the excited electronic state, the DCL does a somewhat better job in reproducing the spectrum (panels (a) and (b) in Fig. 5). Generally, the positions of the individual feature are also given incorrectly in the dynamical classical limit. Here the major origin of the discrepancy should be in the extra term in $\Delta\omega_{\mathrm{DCL}}$.

Regarding general trends which are common for quantum mechanical and dynamical classical spectra, we observe that increasing the temperature results in a less pronounced vibronic structure, since the dephasing rate (and, hence, the width of the vibronic lines) increases with temperature (see Fig. 9 below). Analogously, increasing the difference between ρ_0 and ρ_1 makes the vibronic features broader.

We have also calculated the ACL results for the spectra presented in Fig. 5, which are essentially indistinguishable from the FQM results, and therefore are not shown (see also the discussion of Figs. 6 and 7 below).

We find (see Fig. 10 below) that the worst disagreement between the predictions of FQM and DCL occurs when the coupling strength in the ground electronic state ρ_0 is small compared to ρ_1 (one possible example would involve a nonpolar (in the ground state) molecule, which acquires a large dipole moment upon the electronic excitation). Therefore it would be of interest to test the other approaches to calculating the dipole autocorrelation function (averaged classical

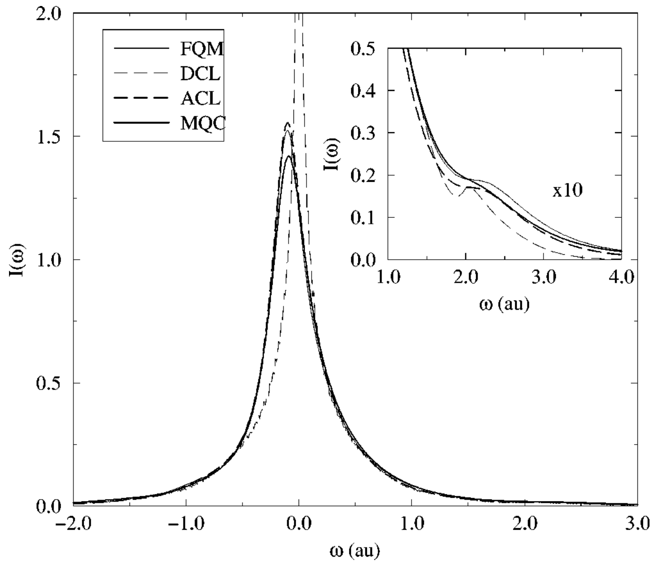

FIG. 6. The electronic absorption spectrum of a diatomic molecule coupled to a harmonic bath. The thin solid, thick solid, thin dashed and thick dashed lines are for FQM, MQC, DCL and ACL results, respectively. The following parameters are used: $\beta = 1$, $\omega_0 = \omega_1 = 1$, $\rho_0 = 0$, $\rho_1 = 0.125$ and we set the shifts in the equilibrium positions to 0. As discussed in the text, the DCL spectrum is centered at $\omega = 0$ (no frequency shift), and its width is too small. The MQC and ACL spectra are in good agreement with the FQM spectrum. The inset emphasizes the presence of the phonon sideband in the blue wing of the absorption spectrum.

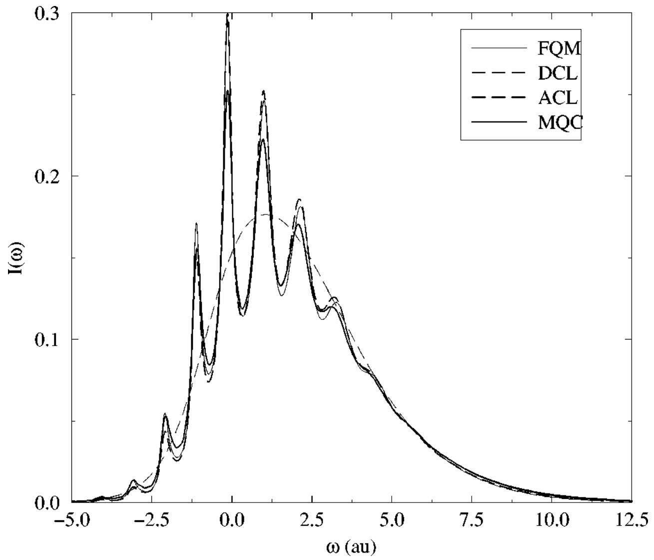

FIG. 7. The electronic absorption spectrum of a diatomic molecule coupled to a harmonic bath. The thin solid, thick solid, thin dashed and thick dashed lines are for FQM, MQC, DCL and ACL results, respectively. The following parameters are used: $\beta = 1$, $\omega_0 = \omega_1 = 1$, $\rho_0 = 0$, $\rho_1 = 0.125$ and we set the shifts in the equilibrium positions to 2. The DCL result reproduces the envelope of the absorption spectrum, but fails to provide the vibronic structure. The MQC and ACL calculation for the absorption spectrum are in good agreement with the FQM result.

and mixed quantum-classical limits) precisely in this situation.

In Fig. 6 we plot the absorption spectra for FQM, DCL, ACL and MQC for the following set of parameters: $\beta = 1$, $\omega_0 = \omega_1 = 1$, $\rho_0 = 0$, $\rho_1 = 0.125$ and we also set $q_1 = 0$. In the absence of ''shifts'' in the equilibrium positions, the dipole autocorrelation function is entirely given by the exponential of the ''rotation'' term (see Section III for details). A technical issue must be addressed at this point: we observe that at long times, both real and imaginary parts of the MQC ''rotation'' term depend linearly on time, which is in agreement with the asymptotic long time behavior obtained in the previous section. Therefore, in order to obtain a converged spectra, we use a linear extrapolation of these functions for long times (the actual MQC calculation is limited by the number of time slices). The time step in the MQC calculation was set to 0.035 a.u. which was found small enough to reproduce within a very good accuracy the FQM spectrum, when the bath position autocorrelation functions, $\chi_\alpha(t)$, in the influence functional (Eq. (61)), were taken quantum mechanically. We therefore use the same time step in the MQC calculation, which was done by replacing the quantum bath correlation functions with their classical counterparts (Eq. (65)).

The best agreement is observed between the FQM and ACL results. This is to be expected on the grounds of Eqs. (20) and (21). For the present problem, in the case $\omega_0 = \omega_1$, the expansion in powers of $\hbar$ of the propagator in Eq. (21) contains only those terms which are retained in the semiclassical approximation. This is the case, since the arithmetic averaged Hamiltonian (cf. Eq. (23)) contains only quadratic terms, and the difference between the ground and excited state Hamiltonians ((cf. Eq. (18)) contains only bilinear terms in the primary oscillator and bath modes. However, the small discrepancy between the two spectra arises due to replacing the quantum thermal averaging with its classical counterpart. As expected, the DCL spectrum (dashed line) is centered at $\omega = 0$ (no frequency shift), and its width is too small (no pure dephasing in the sense of exponential decay). The MQC result is in good agreement with the FQM spectrum both in terms of the shift and the width (the latter is slightly overestimated).

We draw the attention to the phonon sideband in the blue wing of the spectrum shown in the inset. Its shape and relative intensity is determined by the short time dependence of the dipole autocorrelation function, which is fairly similar in all four cases. As such, this feature appears in all four spectra.

In Fig. 7 we plot the absorption spectra for FQM, DCL, ACL and MQC for the same set of parameters as in Fig. 6, but now we have set the shift in the equilibrium position $q_1 = 2$. The DCL reproduces the envelope of the absorption band, but fails to capture any vibronic structure. The MQC captures the vibronic structure but very slightly overestimates the width of the individual lines. The ACL is essentially indistinguishable from the FQM results.

In the case of different frequencies of the primary oscillator in the ground and excited electronic states, the truncation of the expansion in powers of $\hbar$ at the semiclassical level for ACL is no longer exact. Therefore, we have calculated the absorption spectra for FQM, DCL, ACL and MQC for the following set of parameters: $\omega_0 = 1$ and $\omega_1 = \sqrt{1/2}$,

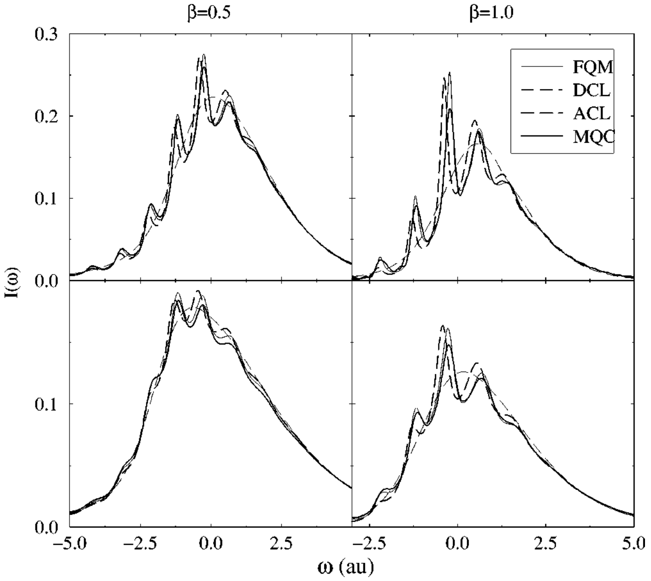

FIG. 8. Plots of the electronic absorption spectrum of a diatomic molecule coupled to a harmonic bath for two different temperatures ($\beta=0.5$ and $\beta=1$). The thin solid, thick solid, thin dashed and thick dashed lines are for FQM, MQC, DCL and ACL results respectively. In order to have the same vertical scale for all panels, we normalized the high temperature spectra to unity, whereas the lower temperature spectra were normalized to half. The ground state coupling strength (ρ_0) in all panels is set to 0. The top and bottom panels are for coupling strength ρ_1 of 0.05 and 0.125, respectively. The DCL absorption spectrum is structureless, whereas FQM, MQC and ACL results are characterized by a vibronic structure. The MQC and ACL calculation for the absorption spectrum are in good agreement with the FQM result.

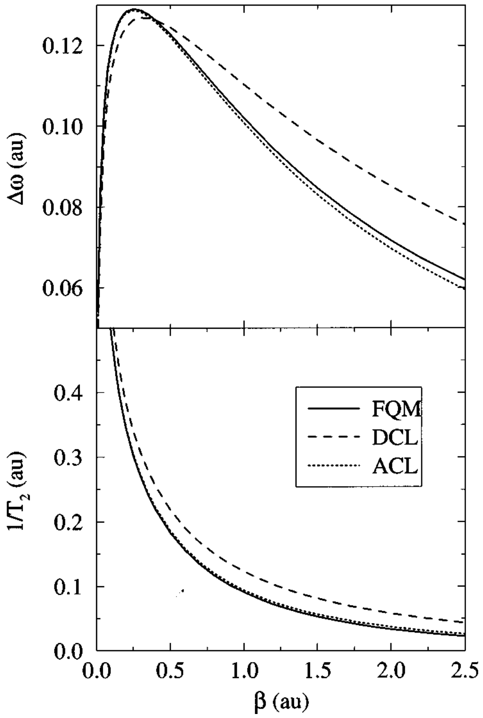

FIG. 9. Plots of temperature dependence of the dephasing rate (bottom panel) $1/T_2$, and the frequency shift (top panel) $\Delta\omega$. Shown are the FQM (solid line), DCL (dashed line) and ACL (dotted line) results for a vibrational frequency $\omega_0=\omega_1=1$, coupling strength $\rho_0=0.125$ and $\rho_1=0.05$, and for a shift in the vibrational equilibrium position of $q_1=2$. A constant value is subtracted from the DCL results for frequency shift to have the same vertical scale as the FQM frequency shift (see Eq. (79) for more details).

for inverse temperatures $\beta=0.5$ and $\beta=1$), and for each value of β—for two values of coupling strength ρ_1 (ρ_0 is kept equal to zero). The results are plotted in Fig. 8. Once again, DCL captures only the envelope, but not the vibronic structure. Contrary to that ACL provides a good approximation to the absorption spectra, albeit somewhat misplaces the positions of individual lines. However, the width is in excellent agreement with FQM results. The best overall agreement is obtained using the MQC approximation, which captures the position and slightly overestimates the width of the individual lines.

To study the long time asymptotic behavior of $C(t)$ as a function of the various parameters, we have calculated the frequency shifts and the dephasing rates for FQM, DCL and ACL from the equations given in the previous section. We first present the results (Fig. 9) for the temperature dependence for a particular set of coupling strengths ($\rho_0=0.125$ and $\rho_1=0.05$) and diatomic vibrational frequencies ($\omega_0=\omega_1=1$). All dephasing rates increase monotonically with temperature. As expected, the agreement between DCL and FQM gets better at higher temperatures. Regarding the frequency shifts, all results display a non-monotonic behavior as functions of temperature. Note that we have subtracted from $\Delta\omega_{\mathrm{DCL}}$ the temperature independent term which arises due to the ''shifts'' in the equilibrium positions (the first term in Eq. (79)). For this particular set of parameters, the ACL results for the dephasing rates and for the frequency shift are in excellent agreement with FQM, since the diatomic vibrational frequencies are the same in the two electronic states. The small discrepancy can be traced to the difference in the thermal probability used to perform the averaging.

In order to study the dependence of the dephasing rate and the frequency shift on the coupling strength, we have calculated $\Delta\omega$ and $1/T_2$ as functions of coupling strength in the ground state ρ_0 for fixed values of temperature ($\beta=1$) and coupling strength in the excited state ($\rho_1=0.125$); again we set the values of ω_0 and ω_1 equal to unity. The results are shown in Fig. 10. We have again subtracted the term due to ''shifts'' from $\Delta\omega_{\mathrm{DCL}}$ (this term is independent of ρ_0). As such, the frequency shifts become zero when $\rho_0=\rho_1$. For $\rho_0<\rho_1$ the frequency shifts are negative, while for $\rho_0>\rho_1$ they are positive. Over a wide range of ρ_0 there is a good agreement between $\Delta\omega_{\mathrm{FQM}}$ and $\Delta\omega_{\mathrm{DCL}}$. However, this agreement breaks down for very low values of ρ_0. In fact for $\rho_0=0$ we have $\Delta\omega_{\mathrm{DCL}}=0$, while the quantum mechanical result approaches a non-zero value. As expected, the ACL results are again in excellent agreement with FQM. For $\rho_0=0$ we have also calculated the MQC result (filled circle in upper panel of Fig. 10), which turns out to be in excellent agreement with the FQM value.

Similar to the frequency shifts, all the dephasing rates vanish when $\rho_0=\rho_1$, i.e., there is no pure dephasing when

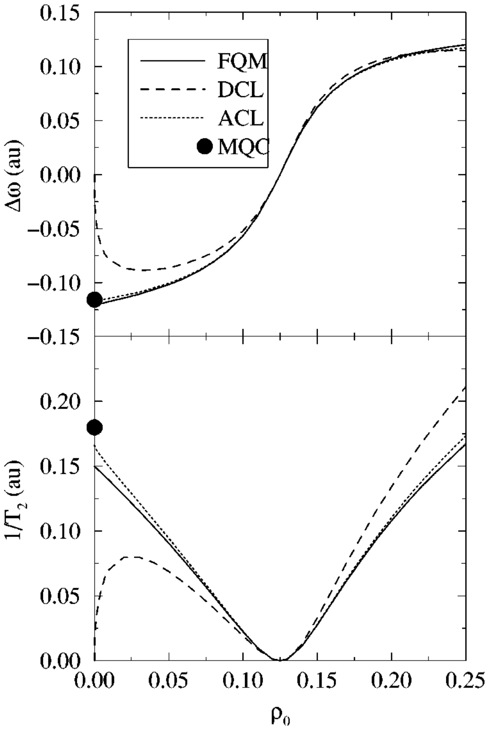

FIG. 10. Plots of the coupling strength (ρ_0) dependence of the dephasing rate (bottom panel) $1/T_2$, and the frequency shift (top panel) $\Delta\omega$. The solid, dashed and dotted lines are the FQM, DCL and ACL results, respectively, and the filled circle (●) is the MQC result for $\rho_0 = 0$. The parameters used are: $\beta = 1$, vibrational frequency $\omega_0 = \omega_1 = 1$, coupling strength $\rho_1 = 0.125$, and for a shift in the vibrational equilibrium position of $q_1 = 2$. A constant value is subtracted from the DCL results for frequency shift to have the same vertical scale as the FQM frequency shift (see Eq. (79) for more details). Note the sudden change in the dephasing rate and in the frequency shift, for DCL at low values of ρ_0 (see text for more details).

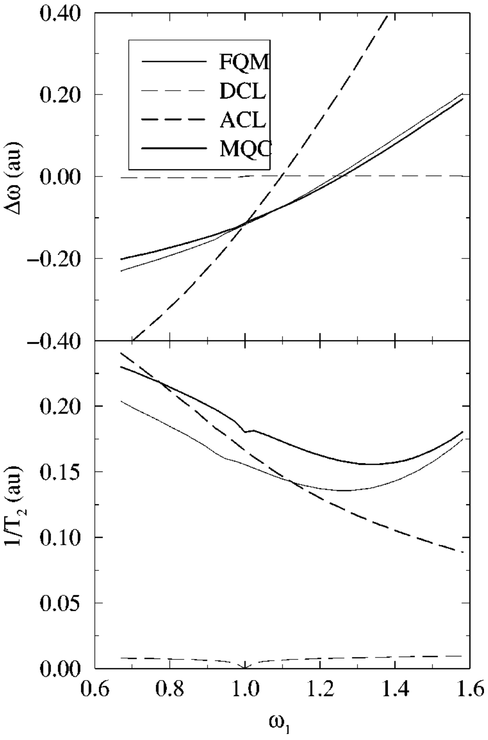

FIG. 11. Plots of the diatomic vibrational frequency (ω_1) dependence of the dephasing rate (bottom panel) $1/T_2$, and the frequency shift (top panel) $\Delta\omega$. The thin solid, thin dashed, thick dashed and thick solid lines are the FQM, DCL, ACL and MQC results respectively. The parameters used are: $\beta = 1$, vibrational frequency $\omega_0 = 1$, coupling strengths $\rho_0 = 0$ and $\rho_1 = 0.125$, and for a shift in the vibrational equilibrium position of $q_1 = 2$. We have subtracted the first term in Eq. (79) from the DCL results for the frequency shift to have the same vertical scale as the frequency shift for the other results (see Eq. (79) for more details).

the coupling in the two electronic states is the same. As the absolute difference in the coupling strength increases, the dephasing rates increase. Overall, there is a reasonable agreement between $1/T_2^{\mathrm{FQM}}$ and $1/T_2^{\mathrm{DCL}}$ except for very low values of ρ_0, where the two results deviate significantly. At $\rho_0 = 0$ the quantum mechanical result approaches a non-zero value, while the DCL dephasing rate vanishes, i.e., the DCL dipole autocorrelation function does not decay exponentially. This has serious consequences for the absorption spectrum, which was illustrated above. The ACL result captures the dephasing rates for the whole range of coupling strengths. To complete the picture we have also plotted (filled circle) the MQC dephasing rate for $\rho_0 = 0$, which is slightly larger than the FQM value.

Finally, in Fig. 11 we plot the frequency shifts and dephasing rates as a function of the diatomic vibrational frequency (ω_1) in the excited electronic state. The following set of parameters are used: $\omega_0 = 1$, $\beta = 1$, $\rho_0 = 0$ and $\rho_1 = 0.125$. By far the best performance is displayed by MQC, which provides a very good approximation to the FQM results. As discussed above, the ACL is not expected to give good results when the difference between the ground and excited diatomic vibrational frequencies is large. This indeed is case, as can be seen in Fig. 11. The worst agreement is between the predictions of DCL and FQM. Note that we have subtracted the first term in Eq. (79) from the DCL results for the frequency shift to have the same vertical scale as the frequency shift for the other results (see Eq. (79) for more details). Adding this term would make the results much worse.

In summary when the coupling strength for the ground electronic state is weak, it is necessary to treat the primary oscillator (diatomic vibrational mode) quantum mechanically, while the bath modes can be treated in the dynamical classical limit. This seem to contradict the conclusions reached by Bader and Berne,[32] and by Egorov and Berne[33] according to which the fully classical treatment is superior to the mixed one in the context of vibrational relaxation. However, for the present problem, the decay of the real-time dipole autocorrelation function is completely dominated by the electronic dephasing process, and not by the vibrational relaxation process. In cases where the vibrational relaxation rate become comparable to the electronic dephasing rate, we anticipate that the MQC will break down. Presumably this could happen when the coupling strengths in both electronic states are large, but the difference between the coupling strengths is small.

VI. CONCLUSIONS

In this paper we have studied the vibronic absorption spectrum of a diatomic molecule (taken in the harmonic approximation) bilinearly coupled to a harmonic bath (with *different* equilibrium positions, coupling strengths, and molecular vibrational frequencies for the two electronic states), in order to test some commonly used semiclassical approximations. We adapted the method of Kubo and Toyozawa to obtain the FQM result for the vibronic absorption spectrum, and provided an alternative treatment based on the path integrals, and present the corresponding influence functional for the problem at hand. The path integral formulation, unlike the method of Kubo and Toyozawa, is not limited to a finite number of bath modes and can be used to treat anharmonic systems.

We also derive analytical expression for the real-time dipole autocorrelation functions in the DCL, ACL, and MQC approximations. Guided by the theory of Hsu and Skinner we obtain the long time behavior of the FQM, DCL and MQC dipole autocorrelation functions, which determines the frequency shifts and the dephasing rates. Our results can be summarized as follows.

(1) The DCL provides a realistic approximation for the dephasing rate, for a wide range of temperatures and coupling strength. However, for low temperatures and for very small values of the coupling strength in the ground electronic state this approximation breaks down (this situation would be observable for a molecule whose ground state is non-polar and the excited state is polar). The frequency shifts calculated in the DCL fail to provide a reasonable approximation to the FQM results.

(2) In most cases studied herein, the DCL provides a qualitative description of the vibronic absorption spectrum. However, the positions of the individual vibronic features and their widths are wrong. Due to the presence of an additional non-exponential component in the decay of the dipole autocorrelation function, the width of the vibronic features are typically broader. As the system-bath coupling strength in the ground electronic state decreases, the performance of the DCL deteriorates significantly.

(3) In the case of pure classical nuclear dynamics we found that ACL provides excellent results for the absorption spectra (for the same diatomic vibrational frequencies in both electronic states), much better than the results obtained using DCL. This is not the case for the system studied by Shemetulskis and Loring,[16] where the dynamical corrections to the inhomogeneously broadened line shape are small, and the choice of the propagation scheme plays a minor role. In the case of different diatomic vibrational frequencies in the two electronic states, as expected, we find discrepancy between ACL and FQM results.

(4) For the cases of small coupling in the ground electronic state and for different frequencies of the primary oscillator in the two electronic states, where the DCL does poorly, and the ACL is not exact, we have obtained excellent agreement between the MQC and the FQM results. This implies that one should treat the primary mode (diatomic vibrational) quantum mechanically and restrict the classical treatment to the bath modes only. Since the primary mode is highly perturbed by the electronic transition, the superior performance of the MQC results in not unexpected.

(5) When the vibrational relaxation rates of both electronic states becomes comparable to the electronic dephasing rate, we anticipate[32] that MQC will deviate from FQM. In practice this situation can occur, since the electronic dephasing rate depends on the difference between the coupling strengths in the two electronic states, whereas the vibrational relaxation rates depend on the magnitude of the couplings.

This work aims to examine the validity of various approximations to obtain the vibronic absorption spectrum in condensed phases. For this reason we have limited ourselves to the case of fully quadratic Hamiltonians; the study of anharmonic systems will be the subject of future investigations.[52] To summarize our results, we have illustrated that for the pure classical treatment of the nuclear degrees of freedom, propagation on the arithmetic averaged Hamiltonian is better than the ground state propagation. However, when non-adiabatic electronic transitions are important, we anticipate that this averaged propagation scheme will fail when the two Hamiltonians differ significantly.[53] We find that the overall best performance is given by the MQC approximation, which presumably would break down when vibrational relaxation rates become comparable to the electronic dephasing rate.

The treatment of realistic systems requires additional approximations. The choice of the propagation scheme for the quantum part of the system and the choice of the method for propagating quantum and classical degrees of freedom together are still open questions for future study.

ACKNOWLEDGMENTS

This work was supported by a grant to B.J.B from the National Science Foundation. E.R. is a Rothschild and Fulbright post-doctoral fellow.

APPENDIX: THE INFLUENCE FUNCTIONAL

In this Appendix we provide the generalization of the influence functional obtained by Feynman and Vernon[44] for the present problem. We adopt the notation of Wolynes and collaborators[47] and write the influence functional as a product of three terms:

$$I(q^+,q^-,q,t)=I_t(q^+,q^-,t)I_\beta(q)I_C(q^+,q^-,q,t). \quad \text{(A1)}$$

The three terms arise because there are three types of influence functional bonds: those that connect two points in real time (I_t), those that connect two points in imaginary time (I_β), and those which connect real-time points to imaginary-time points (I_C). For I_t we obtain

$$I_t(q^+,q^-,t)=\exp\left\{-\frac{1}{\hbar^2}\int_0^t dt_1\int_0^{t_1} dt_2 q^+(t_1)q^+(t_2)\right.$$

$$\left.\times\sum_\alpha^{N_b}(g_\alpha^0)^2\chi_\alpha(t_1-t_2)-q^+(t_1)q^-(t_2)\right.$$

$$\times\sum_{\alpha}^{N_b} (g_\alpha^0 g_\alpha^1)\chi_\alpha^*(t_1-t_2)-q^-(t_1)q^+(t_2)$$

$$\times\sum_{\alpha}^{N_b} (g_\alpha^0 g_\alpha^1)\chi_\alpha(t_1-t_2)+q^-(t_1)q^-(t_2)$$

$$\left.\times\sum_{\alpha}^{N_b} (g_\alpha^1)^2\chi_\alpha^*(t_1-t_2)\right\}, \tag{A2}$$

where q^+ and q^- are the forward and backward path, respectively (see also Section III C for more details). The imaginary time path is given by

$$I_\beta(q)=\exp\left\{\frac{1}{2\hbar^2}\int_0^{\beta\hbar}d\tau_1\int_0^{\beta\hbar}d\tau_2 q(\tau_1)q(\tau_2)\right.$$

$$\left.\times\sum_{\alpha}^{N_b} (g_\alpha^0)^2\chi_\alpha(i(\tau_1-\tau_2))\right\}, \tag{A3}$$

where q is the thermal path. Finally, for the real-time points to imaginary-time points we find

$$I_C(q^+,q^-,q,t)$$

$$=\exp\left\{\frac{i}{\hbar^2}\int_0^t dt_1\int_0^{\beta\hbar}d\tau q^+(t_1)q(\tau)\right.$$

$$\times\sum_{\alpha}^{N_b} (g_\alpha^0)^2\chi_\alpha(t_1-i(\beta\hbar-\tau))-q^-(t_1)q(\tau)$$

$$\left.\times\sum_{\alpha}^{N_b} g_\alpha^0 g_\alpha^1\chi_\alpha(t_1-i(\beta\hbar-\tau))\right\}. \tag{A4}$$

In the above $\chi_\alpha(t_1-t_2)=\langle Q_\alpha(t_1)Q_\alpha(t_2)\rangle$ is the real-time bath position autocorrelation function

$$\chi_\alpha(t_1-t_2)=\frac{\hbar}{2\omega_\alpha}\{\coth[\beta\hbar\omega_\alpha/2]\cos(\omega_\alpha(t_1-t_2))$$

$$-i\,\sin(\omega_\alpha(t_1-t_2))\}. \tag{A5}$$

[1] *Spectroscopy and Excitation Dynamics of Condensed Molecular Systems* edited by V. M. Agranovich and R. M. Hochstrasser (North-Holland, Amsterdam, 1983).

[2] S. Mukamel, *Principles of Nonlinear Optical Spectroscopy* (Oxford University Press, Oxford, 1995).

[3] J. L. Skinner and W. E. Moerner, J. Phys. Chem. **100**, 13251 (1996).

[4] D. Thirumalai and B. J. Berne, Comput. Phys. Commun. **63**, 415 (1990).

[5] D. Chandler, in *Liquids, Freezing and Glass Transition*, edited by D. Levesque, J.-P. Hansen, and J. Zinn-Justin (North-Holland, Amsterdam, 1991), Chap. 4., pp. 193–285.

[6] J. E. Gubernatis, M. Jarrell, R. N. Silver, and D. S. Sivia, Phys. Rev. B **44**, 6011 (1991).

[7] E. Gallicchio and B. J. Berne, J. Chem. Phys. **105**, 7064 (1996).

[8] D. Kim, J. D. Doll, and J. E. Gubernatis, J. Chem. Phys. **106**, 1641 (1997).

[9] C. E. Creffield, E. G. Klepfish, E. R. Pike, and S. Sarkar, Phys. Rev. Lett. **75**, 517 (1995).

[10] S. A. Egorov, E. Gallicchio, and B. J. Berne, J. Chem. Phys. **107**, 9312 (1997).

[11] R. B. Gerber and M. A. Ratner, Adv. Chem. Phys. **74**, 97 (1988).

[12] D. G. Evans and R. D. Coalson, J. Chem. Phys. **97**, 5081 (1992).

[13] A. Nitzan and R. J. Silbey, J. Chem. Phys. **60**, 4070 (1974).

[14] S. Mukamel, J. Chem. Phys. **77**, 173 (1982).

[15] L. E. Fried and S. Mukamel, J. Chem. Phys. **96**, 116 (1992).

[16] N. E. Shemetulskis and R. F. Loring, J. Chem. Phys. **97**, 1217 (1992).

[17] J. G. Saven and J. L. Skinner, J. Chem. Phys. **99**, 4391 (1993).

[18] A. Heidenreich and J. Jortner, J. Chem. Phys. **105**, 8523 (1996).

[19] P. Pechukas, Phys. Rev. **181**, 166 (1969).

[20] P. Pechukas, Phys. Rev. **181**, 174 (1969).

[21] J. C. Tully, Surf. Sci. **299/300**, 667 (1994).

[22] P. J. Rossky, J. Opt. Soc. Am. B **7**, 1727 (1990).

[23] F. J. Webster, J. Schnitker, M. S. Friedrichs, R. A. Friesner, and P. J. Rossky, Phys. Rev. Lett. **66**, 3172 (1991).

[24] B. J. Schwartz and P. J. Rossky, J. Chem. Phys. **105**, 6997 (1996).

[25] D. F. Coker, in *Computer Simulation in Chemical Physics*, edited by M. P. Allen and D. J. Tildesley (Kluwer, Dordrecht, 1993), pp. 315–377.

[26] L. Xiao and D. F. Coker, J. Chem. Phys. **199**, 8646 (1994).

[27] M. Ben-Nun, R. D. Levine, and G. R. Fleming, J. Chem. Phys. **105**, 3035 (1996).

[28] D. Thirumalai, E. J. Bruskin, and B. J. Berne, J. Chem. Phys. **83**, 230 (1985).

[29] E. J. Heller, J. Chem. Phys. **62**, 1544 (1975).

[30] E. J. Heller, Acc. Chem. Res. **14**, 268 (1981).

[31] M. F. Herman, Annu. Rev. Phys. Chem. **45**, 83 (1994).

[32] J. S. Bader and B. J. Berne, J. Chem. Phys. **100**, 8359 (1994).

[33] S. A. Egorov and B. J. Berne, J. Chem. Phys. **107**, 6050 (1997).

[34] J. L. Skinner and D. Hsu, J. Phys. Chem. **90**, 4931 (1986).

[35] D. Hsu and J. L. Skinner, J. Lumin. **37**, 331 (1987).

[36] B. DiBartolo, *Optical Interactions in Solids* (Wiley, New York, 1968).

[37] J. E. Straub, M. Borkovec, and B. J. Berne, J. Phys. Chem. **91**, 4995 (1987).

[38] R. G. Gordon, Adv. Magn. Reson. **3**, 1 (1968).

[39] A. L. Fetter and J. D. Walecka, *Quantum Theroy of Many-Particle Systems* (McGraw–Hill, New York, 1971).

[40] M. Hillery, R. F. O'Connell, M. O. Scully, and E. P. Wigner, Phys. Rep. **106**, 121 (1984).

[41] R. Kubo and Y. Toyozawa, Prog. Theor. Phys. **13**, 160 (1955).

[42] R. Balian and E. Brezin, Nuovo Cimento B **64**, 37 (1969); R. W. Munn and R. Silbey, J. Phys. A: Math. Gen. **11**, 939 (1978).

[43] M. Lax, J. Chem. Phys. **20**, 1752 (1952).

[44] R. P. Feynman and F. L. Vernon, Ann. Phys. **24**, 118 (1963).

[45] A. Nitzan and B. N. J. Persson, J. Chem. Phys. **83**, 5610 (1985).

[46] R. A. Harris, R. A. Mathies, and W. T. Pollard, J. Chem. Phys. **85**, 3744 (1986).

[47] R. E. Cline, Jr. and P. G. Wolynes, J. Chem. Phys. **88**, 4334 (1988).

[48] R. P. Feynman and A. R. Hibbs, *Quantum Mechanics and Path Integrals* (McGraw-Hill, New York, 1965).

[49] L. S. Schulman, *Techniques and Applications of Path Integration* (Wiley, New York, 1981).

[50] N. Makri, Chem. Phys. Lett. **193**, 435 (1992).

[51] J. Cao, L. W. Ungar, and G. A. Voth, J. Chem. Phys. **104**, 4189 (1995).

[52] E. Rabani, S. A. Egorov, and B. J. Berne (unpublished).

[53] J. C. Tully, J. Chem. Phys. **93**, 1061 (1990).